Abnormal Detection Line Method to Estimate Disconnection Points in Power Distribution Lines

Yasuhiro Kodama and Yasuhiro Hayashi, *Member, IEEE*

***Abstract*—Natural phenomena such as gale, rain, and lightning cause disconnections, which can disrupt power distribution. Therefore, a method that can estimate the disconnection point (DP) in power distribution lines is needed to ensure public safety and a stable power supply. A simple DP detection method using a common earthing conductor is applied to both residential and industrial areas with only two distribution lines with interconnection points at the ends. However, this method cannot be used in rural areas that have distribution lines without interconnection points. Therefore, we propose a novel DP estimation method for use in distribution lines in rural areas. To this end, an abnormal detection line was installed along a long distribution line with branch lines and ammeters placed at its starting and end points. DP estimation was realized by calculating the time difference between the zero-crossing points of the current flowing in the two ammeters. The DP estimation effectiveness of the proposed method was validated by simulating long distribution lines. Thus, the proposed method can be used to improve the performance of the distribution lines in rural areas.**

***Index Terms*—Abnormal detection line, disconnection point, disconnection point estimation methods, DP estimation, time difference of the zero-crossing point, distribution line, disconnection point estimation in rural areas.**

Nomenclature

DP	disconnection point
ADL	abnormal detection line
AI	artificial intelligence
ATP	Alternative Transient Program
ITSW	information technology switchgear
VS	voltage sensor

I. Introduction

POWER-SUPPLY disturbances in distribution lines are attributed to ground faults, short circuits, and disconnections. Since 2010, over 10000 incidents of power-supply disruptions have been reported in Japan [1]. Ground faults, which are caused by contact with birds, animals, and trees, are identified as the primary cause of power disruptions. Methods such as wavelet analysis [2], fast Fourier transform analysis [3], methods based on common earthing conductors [4], and artificial neural networks [5] have been developed to estimate ground-fault points in distribution lines.

For short-circuit point estimation, methods such as pulse injection [6] and the method using anomaly-detection lines proposed by the author [7] have been studied.

In this study, we considered natural phenomena such as gale, rain, lightning, ice, snow, and tree contact as primary causes of disconnection. If a disconnected high-voltage line is connected to the grounding band at the time of disconnection, it develops into a ground fault and terminates the power supply to the distribution line. In contrast, the disconnection may not lead to a ground fault if the conductor of the high-voltage line is coated; the wire coating would cover the conductor after the disconnection. The protection relay of the distribution line does not operate under the disconnected state, and the power supply is not interrupted. If a person encounters a disconnected distribution line, there is a high risk of an electric shock. Thus, early detection of the disconnection point (DP) is necessary to ensure safety.

Various DP estimation methods have been reported using smart meters [8], artificial intelligence (AI) [9], and common earthing conductors [10], [11]. Moreover, extensive studies have been conducted to determine the voltage characteristics of the measuring equipment installed on a distribution line [12], [13], [14]. Further, several methods have been proposed to estimate the DPs in one branch of a distribution line by mining the system characteristics from the multisource data of distribution lines [15] and using machine learning with power, voltage, and current data [16]. Studies on the operation of relays depending on failure at the time of disconnection are underway [17].

DP estimation methods that employ smart meters are effective for urban and residential areas. In these methods, smart meters are installed across distribution lines; however, in rural areas, limited consumers are scattered across electricity-demand locations, and therefore it is difficult to identify the DP at the time of disconnection in the distribution line that connects the demand locations of users with no electricity.

In AI-based DP estimation methods, the DP is estimated considering the changes in the voltage and current waveforms generated at the time of disconnection. To determine the voltage

Manuscript received 15 September 2022; revised 4 January 2023; accepted 19 February 2023. Date of publication 23 February 2023; date of current version 25 July 2023. Paper no. TPWRD-01364-2022.

The authors are with the Advanced Collaborative Research Organization for Smart Society, Waseda University, Tokyo 162-0041, Japan (e-mail: yasukoda067@aoni.waseda.jp; hayashi@waseda.jp).

Color versions of one or more figures in this article are available at https://doi.org/10.1109/TPWRD.2023.3248532.

Digital Object Identifier 10.1109/TPWRD.2023.3248532

characteristics, the DP is specified by the number of voltage sensors installed. Further, a simple method is required to estimate the DP using data mining. Similarly, in the machine learning approach, a method that does not require a complex analysis of power, voltage, and current data is necessary. As described in [14], there are limited studies on the disconnection of distribution lines. Therefore, novel detection methods need to be developed to ensure public safety and a stable supply of electricity.

Current DP estimation methods focus on the trunk and branch lines of the distribution system [10], [11]. Ammeters are mounted at the starting point of a common earthing conductor installed on two adjacent distribution lines, and the DP is estimated by detecting the change in the phase of the current flowing through the ammeters at the time of disconnection. In this method, two adjacent distribution lines are considered in residential and urban areas. Unlike the method described in [10], [11], the DP must be identified within a narrow region using information from ammeters installed at the starting and end points of the common earthing conductor in rural areas. Therefore, there is a need for further improvement and validation of this method to apply it to distribution lines in rural areas.

In this study, we propose a DP estimation method considering a long distribution line that does not include interconnection points with other distribution lines common in rural areas. The proposed method involves installing an abnormal detection line (ADL) that detects the difference in the current flowing in the high-voltage line before and after a disconnection in the distribution line. In addition, grounding electrodes are installed at the starting and end points of the ADL. The proposed method estimates the DP based on the time difference between the zero-crossing points of the current flowing through the ammeters installed on the ADL during the disconnection.

The rest of this manuscript is organized as follows: Section II describes the current distribution line disconnection phenomenon, and Section III presents the proposed methodology and its theory. Section IV presents the simulation model and results, which are analyzed in further detail in Section V. Section VI discusses the validity of the theory of the proposed method, the advantages of the proposed method, and an application example where the proposed method is utilized at a real site. Finally, conclusions are provided in Section VII.

II. Current Distribution Line Disconnection Phenomenon

Fig. 1 illustrates several distribution lines originating from one distribution substation with a grounding resistance (NGR) of 10 kΩ, which is equivalent to high-resistance grounding. Fig. 2 displays three high-voltage lines, the ADL, the transformer, and the switchgear located on the utility pole. The ground voltage of each phase of the high-voltage lines is 3.81 kV, and the line-to-line voltage is 6.6 kV. Fig. 3 shows the electricity supply to high-voltage consumers at 6.6 kV and to households at 6.6 kV to 100/200 V or 6.6 kV to 200 V for low-voltage consumers with large capacities.

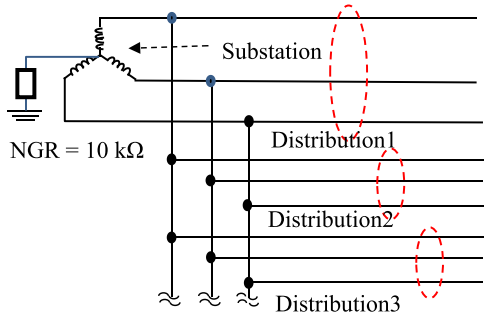

Fig. 1. Distribution line connection.

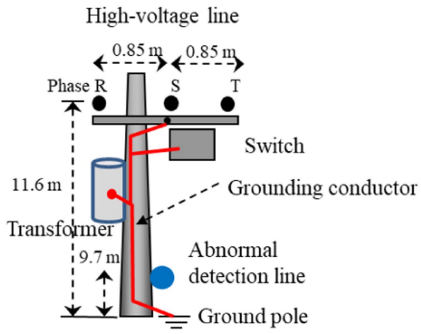

Fig. 2. Placement of wires and equipment on the utility pole.

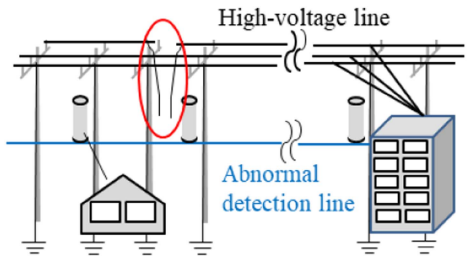

Fig. 3. Schematic of power supply distribution from distribution lines to high- and low-voltage consumers.

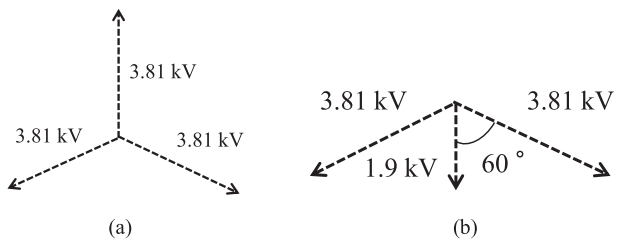

Fig. 4. Voltage vector before and after disconnection. (a) Before disconnection. (b) After disconnection.

During disconnection, the voltages of the two non-disconnected phases remain unchanged. The voltage of the disconnected phase after the disconnection is half of its original magnitude; its phase changes by 180° compared with that before the disconnection. Fig. 4 shows a vector diagram of the voltage characteristics before and after the disconnection.

Currently, there is a difference in the disconnection detection process on the trunk and branch distribution lines because automatic switches are installed on the trunk, and no such switches are installed on the branch. For trunk line disconnection, the presence or absence of disconnection can be confirmed based on variations in the voltage phase before and after the disconnection using an automatic switch; however, the DP cannot be identified. Disconnection in the branch line is difficult to detect because the trunk line voltage remains unchanged following the disconnection.

III. Proposed Method and Theory of Proposed Method

A. Proposed Method

In the proposed method, ammeters are installed at the starting and end points of the ADL to measure the current before and after disconnection. The DP is estimated by detecting the time difference between the zero-crossing points of the currents flowing in the two ammeters before and after the disconnection. The distribution lines in rural areas are long and installed away from the substation to the scattered demand areas; therefore, the establishment of interconnection points with other distribution lines is difficult. In this study, we propose a DP estimation method for a single distribution line using an ADL.

The difference between the proposed and existing methods includes the use of an ADL instead of a common earthing conductor. The common earthing conductor is connected between adjacent poles and the grounding pole of each electrode, and it is subsequently connected to the adjacent distribution line at the end. Further, in existing methods, the frame of the switchgear, transformer, and grip of the high-voltage distribution lines are connected to the grounding electrode. However, in this study, the ADL was connected only to the grounding poles at the starting and end points of the distribution line.

B. Theoretical Consideration

Fig. 5 illustrates the method proposed in previous studies [10], [11], which estimates the DP from the time difference between the zero-crossing points of the currents measured by ammeters CT1 and CT2 installed at the starting point of each common earthing conductor when a disconnection occurs in a distribution line where the common earthing conductors of two adjacent distribution lines are connected only at their ends. The proposed method estimates the DP based on the time difference between the zero-crossing points of the currents measured at the starting point of a common earthing conductor. Similar to previous studies [10], [11], the change in the synthetic resistance and synthetic inductance of the common earthing conductor related to the disconnection caused by the change in the high-voltage line current after the disconnection are identified as factors that cause the time difference at the zero-crossing point when a disconnection occurs.

In the present study, one distribution line in a rural area was considered under the condition that the ammeters are installed at the starting and end points of the distribution line. We assume that the induced voltage (caused by the product of the mutual

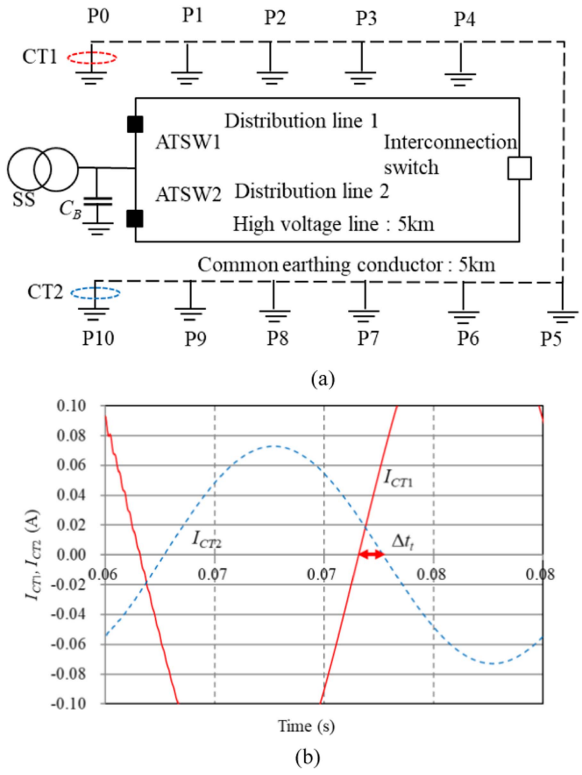

Fig. 5. Conceptual diagram of the method proposed in previous studies. (a) Model distribution line. (b) Time difference between the zero-crossing points of I_{CT1} and I_{CT2}.

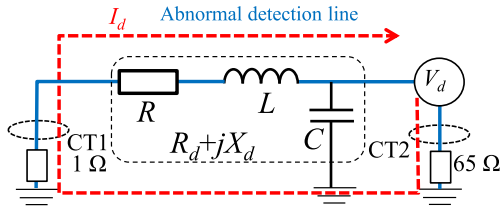

Fig. 6. Equivalent circuit of the abnormal detection line.

inductance of the high-voltage line and ADL, and the zero-phase current of the high-voltage line) in the ADL at the time of disconnection is $V_d = V_{dm}\cos(\omega t+\varphi_1)$, where V_{dm} is the peak value, $\omega = 2\pi f$, and φ_1 is the phase; the current flowing on the power supply side is $I_d = I_{dm}\cos(\omega t+\varphi_2)$, where I_{dm} is the peak value, $\omega = 2\pi f$, and φ_2 is the phase. The equivalent circuit when AC voltage is applied to the RLC circuit is shown in Fig. 6. The distribution substation that supplies power to the distribution line is shown on the left of the figure; the resistance of the distribution substation was set to 1 Ω. The ground resistance of the utility pole depicted in Fig. 2 at the end of the distribution line was set as 65 Ω based on the technical guidelines for lightning protection in Japan, as shown in Fig. 6. CT1 and CT2 were installed as shown in Fig. 6. Here, R_d and X_d represent the resistance and impedance of the ADL, respectively. Therefore, the current flowing into the ADL flows from the right side to the left side of the diagram when a disconnection occurs; the voltage source is shown on the

right side of the diagram. In addition, I_d is obtained by dividing V_d by (R_d+jX_d), where j represents an imaginary number. The time difference between these zero-crossing points is attributed to the changes in X_d and R_d of the ADL, depending on the DP; the time difference between the zero-crossing points of the currents flowing in CT1 and CT2 with respect to the current flowing in CT2 is expressed by [10], [11]

$$\Delta t_d = \frac{\theta_d}{\omega} = \left(\tan^{-1}\frac{X_d}{R_d}\right)/\omega, \tag{1}$$

where θ_d represents the phase difference between V_d and I_d, and $\omega = 2\pi f$ at $f = 50$ Hz. If the ratio of X_d and R_d increases, Δt_d increases. Thus, Δt_d depends on the impedance of the wire applied to the ADL.

X_d and R_d need to be calculated to evaluate Δt_d from (1). X_d and R_d can be obtained from

$$Z_d = \frac{V_d}{I_d} = \frac{V_{dm}}{I_{dm}}(\cos\theta_d + j\sin\theta_d) = R_d + jX_d, \tag{2}$$

However, to calculate (2), θ_d must be obtained from (3), which is obtained by calculating electric power P_d; it is given by

$$P_d = \int_{T_{Ps}}^{T_{Pf}} \frac{V_d \times I_d}{(T_{Pf} - T_{Ps})} dt = \frac{V_{dm} \times I_{dm} \times \cos\theta_d}{2}, \tag{3}$$

where T_{Ps} and T_{Pf} indicate the P_d integration start and end time, respectively. P_d represents the average value of one cycle. R_d and X_d can be obtained by solving (3) for θ_d and substituting it into (2); Δt_d can be calculated by substituting these values into (1).

C. Factors Causing Changes in X_d

In previous studies [10], [11], the change in the impedance of the ADL X_d shown in Fig. 6 was large compared to that in R_d obtained from (2) when a disconnection occurred. Here, X_d is calculated using

$$X_d \approx \omega L_a - 1/\omega C_l \approx \omega L_a, \tag{4}$$

where $\omega = 2\pi f$. L_a represents the acting inductance of the ADL considering the interaction with the high-voltage line, and C_l represents the capacitance between the ADL and ground. C_l should not be considered because the impedance of C_l becomes large (approximately several microfarads per kilometer).

Factors that cause L_a to change before and after the disconnection are examined as follows: L_a is calculated by dividing the sum of the number of magnetic fluxes φ_s of the ADL and the number of magnetic fluxes φ_m attributed to the mutual inductance between the ADL and high-voltage line by I_d; this is calculated using

$$L_a = (\varphi_s + \varphi_m)/I_d, \tag{5}$$

where φ_s represents the product of the self-inductance L_s of ADL and I_d. φ_s is calculated using

$$\varphi_s = L_s \times I_d, \tag{6}$$

φ_m represents the product of each phase of the mutual inductance between the high-voltage line and ADL and high-voltage line current. φ_m is calculated using

$$\begin{aligned}\varphi_m &= L_{m-R} \times I_{h-R} + L_{m-S} \times I_{h-S} + L_{m-T} \times I_{h-T} \\ &= L_m (I_{h-R} + I_{h-S} + I_{h-T}) = L_m \times I_{h0},\end{aligned} \tag{7}$$

TABLE I
MUTUAL INDUCTANCE BETWEEN HIGH-VOLTAGE AND COMMON GROUND LINES

$L_{m\text{-}R}$ (mH)	$L_{m\text{-}S}$ (mH)	$L_{m\text{-}T}$ (mH)
1.24	1.24	1.22

The mutual inductances of the phases of the high-voltage line, R, S, and T, and the ADL are expressed as $L_{m\text{-}R}$, $L_{m\text{-}S}$, and $L_{m\text{-}T}$, respectively; the corresponding currents are $I_{h\text{-}R}$, $I_{h\text{-}S}$, and $I_{h\text{-}T}$, respectively. Here I_{h0} represents the zero-phase current of the high-voltage three-wire line. Table I summarizes the mutual inductance of each phase of the high-voltage line calculated using the line constant calculation program Alternative Transient Program (ATP). Table I indicates that the mutual inductance of each phase of the high-voltage line and the ADL is almost equal, and it can be expressed as L_m. Equations (5)–(7) can be summarized as

$$\begin{aligned}L_a &= (L_s + L_m \times I_{h0}/I_d) \\ &= (L_s + L_m \times I_{h0m}/I_{dm} \times \cos\theta_{hD}) \\ &= (L_s + L_m \times x_i),\end{aligned} \tag{8}$$

By using the maximum values of $I_{h0\,m}$ and I_{dm} in the analysis, the nature of the simulation results for before and after disconnection can be easily understood. x_i in (8) is obtained as follows:

$$\begin{aligned}x_i &= \frac{I_{h0}}{I_d} = \frac{I_{h0} \cdot I_d}{I_d \cdot I_d} = \int_{T_{is}}^{T_{if}} \frac{I_{h0} \cdot I_d}{I_d \cdot I_d} dt \\ &= \frac{I_{h0m} \cdot I_{dm} \cdot \cos\theta_{hD}}{I_{dm} \cdot I_{dm}} = \frac{I_{h0m} \cdot \cos\theta_{hD}}{I_{dm}},\end{aligned} \tag{9}$$

where I_{dm} and I_{h0m} represent the peak values of I_d and I_{h0}, respectively; x_i represents the ratio of I_{dm} and I_{h0m} multiplied by $\cos\theta_{hd}$ obtained from the phase difference between I_{h0} and I_d, so that x_i represents the average value of one cycle; and T_{is} and T_{if} are the start and end time for calculating (9), respectively. From the relationship between (1), (4), and (8), the time difference at the zero-crossing point before and after the disconnection is caused by the change in the magnitude and phase of the zero-phase current in the high-voltage line and the current flowing in the ADL.

IV. Simulation Model and Results

A. Simulation Model

Fig. 7 shows the outline of the distribution-line model. The length of the trunk line is approximately 10 km, which is long, considering that the target distribution line is used in rural areas. The branch lines originate 2 and 8 km away from the feed point of the distribution line; the length of each branch line is 5 km. For the trunk line, the nodes on the distribution-line model denoted

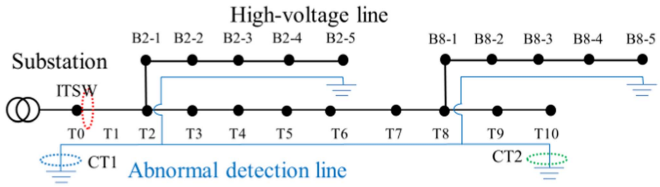

Fig. 7. Simulation model of the distribution line.

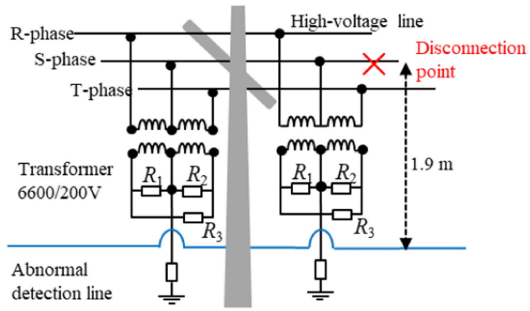

Fig. 8. Transformer wiring diagram.

TABLE II
HIGH-VOLTAGE LINE AND ADL SPECIFICATIONS

R (Ω/km)	Inductance (H/km)	Capacitance (μF/km)
0.297	2.18×10^{-3}	9.45×10^{-3}

by T1 to T10 are located every 1 km from the feed point of the distribution line. Nodes B2-1–B2-5 are located every 1 km from the branch point of the branch line originating at 2 km from the feed point. Nodes B8-1–B8-5 are located every 1 km from the branch point of the branch line originating at 8 km from the feed point. The high-voltage line is a three-phase three-wire system that has loads on the trunk and branch lines every 1 km. Switchgear with built-in sensors, known as information technology switchgear (ITSW), of the high-voltage line was installed at the feed point of the distribution line. An ADL was grounded at the starting and end points of the trunk line and each branch line. Two ammeters (CT1 and CT2) were installed to measure the current flowing at the starting and end points of the ADL. The grounding of the ADL shared the grounding resistance value of 1 Ω with the distribution substation at the starting point of the ADL, and grounding resistance was 65 Ω at the end point of the branch line, according to the lightning protection standards. Fig. 8 depicts that the ADL is installed 1.9 m below the high-voltage line. Table II summarizes the specifications of the high-voltage lines and ADL.

Fig. 8 illustrates that the load of the distribution line is arranged at $R1$, $R2$, and $R3$ to a high-voltage V-connected three-phase transformer in this study. Further, the load under the conditions presented in Table III is set such that the magnitude of the three-phase current is balanced and unbalanced for each phase. The load from P2 to P4 in Table III modifies the resistance value between each phase from 1 Ω to 0.5 Ω. Furthermore, the load is installed on the low-voltage line, which is transformed

TABLE III
SETTING CONDITIONS OF LOAD AND CURRENT VALUES FOR EACH PHASE

	R_1 (Ω)	R_2 (Ω)	R_3 (Ω)	I_R (A)	I_S (A)	I_T (A)
P1	1	1	1	202.7	202.9	205.6
P2	0.5	1	1	202.7	309.1	303.3
P3	1	0.5	1	307.9	298.2	206.5
P4	1	1	0.5	299.0	202.2	312.2

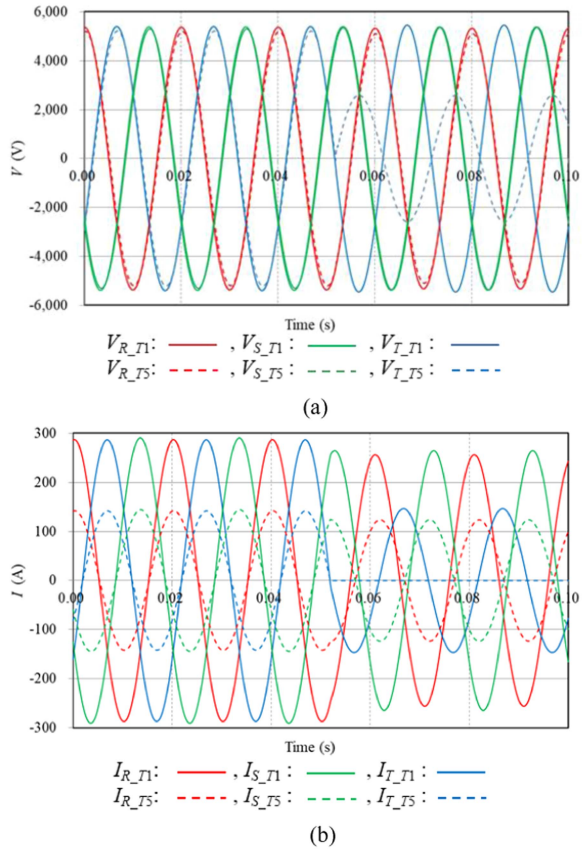

Fig. 9. Voltage and current waveforms on the starting and ending sides of the DP when the trunk line is disconnected at T5. (a) Voltage waveform. (b) Current waveform.

from 6.6 kV to 200 V by the transformer installed on the electric pole.

We used ATP simulation to perform a transient analysis of the power system. In the ATP simulations, we considered the distribution-line model shown in Fig. 7, wherein the disconnection occurs in the trunk and branch lines. The disconnection condition was obtained by setting the disconnected phase as the S-phase (Fig. 8), and the DP was set at every 1 km for the trunk and branch lines. The ATP simulation was performed in the time range 0.0–0.1 s at intervals of 10^{-6} s, with a disconnection occurring at $t = 0.05$ s.

B. Simulation Results

Fig. 9(a) and (b) show the voltage and current waveforms, respectively, considering T1 and T5 of the distribution-line model (Fig. 7) based on load condition P1 (Table III) and

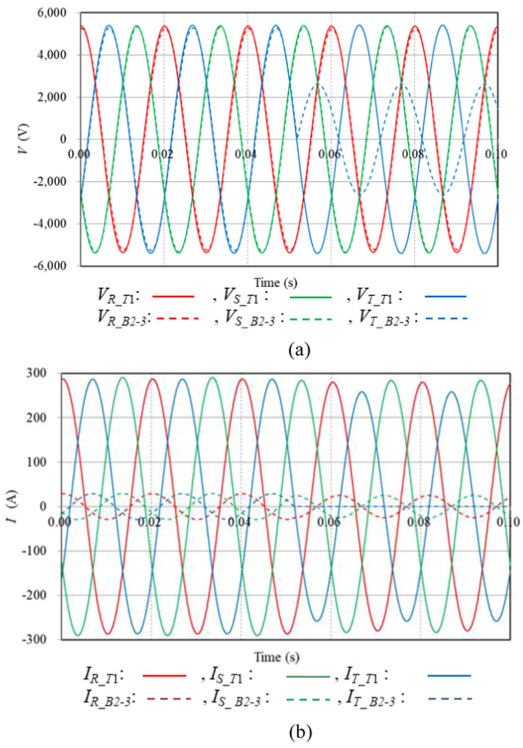

Fig. 10. Voltage and current waveforms at the starting point of the distribution line and end of the DP when the branch wire is disconnected at B2-3. (a) Voltage waveform. (b) Current waveform.

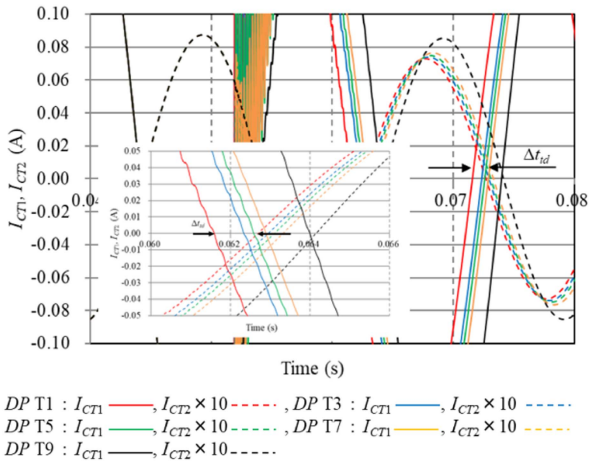

Fig. 11. I_{CT1} and I_{CT2} at the time of trunk line disconnection under condition P1.

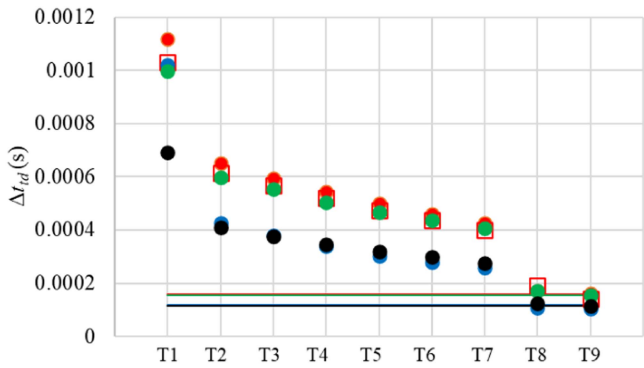

Fig. 12. Disconnection distance dependence of Δt_{td} under condition P1.

disconnection at T5. Waveforms at T1 and T5 are represented by solid and dotted lines, respectively. As indicated in Fig. 9(a), the voltage waveform at T1 remains the same before and after the disconnection because the DP is on the load side of T1. The voltage waveform at T5 confirms that the magnitude of the voltage of the disconnected phase approximately halved and had a phase change of 180° after disconnection. This result is consistent with those in Fig. 4(b), which shows the voltage characteristics at the time of disconnection. Fig. 9(b) illustrates that the current waveform at T1 decreases as the current flowing from the DP to the load side decreases during disconnection. For the current waveform at T5, the current does not flow between the phase associated with the disconnected phase. Consequently, the current flows only to the load connected to the two phases that are not the disconnected phases; this resulted in a single-phase load, and the current exhibited a phase difference of 180°.

Fig. 10 shows the voltage and current waveforms of T1 and B2-3 in the distribution-line model (Fig. 7) at the time of disconnection considering B2-3 under condition P1 (Table III).

Fig. 10(a) indicates that the voltage waveform at T1 is not affected by the disconnection. In the voltage waveform at the load side of B2-3, the voltage of the disconnected phase is approximately halved, and the phase changes by 180°. This result is consistent with Fig. 4(b), which shows the voltage characteristics at the time of disconnection. According to Fig. 10(b), the current supplied to the load side from the DP decreases after the disconnection, which decreases the current flow in the disconnected phase at T1. The current through the disconnected phase at DP B2-3 reaches zero, and the load connected to the two phases that were not disconnected became a single-phase load. Consequently, the current flowing between the two phases exhibited a phase difference of 180°.

In the case of condition P1 (Table III), the DPs were set to T1, T3, T5, T7, and T9. Fig. 11 shows the corresponding simulation results. To ensure that I_{CT1} and I_{CT2} had the same magnitude, I_{CT2} was set to a value 10 times that of the simulation. The phases of the currents I_{CT1} and I_{CT2} changed before and after the disconnection. The time difference between the zero-crossing points of I_{CT1} and I_{CT2} before and after the disconnection is referred to as Δt_{td}; the relationship between Δt_{td} and DPs is illustrated in Fig. 12. For the load conditions summarized in Table III, P1 is –, P2 is –, P3 is –, and P4 is – for Δt_{td} before disconnection, and P1 is •, P2 is •, P3 is •, and P4 is • for Δt_{td} after disconnection. As shown in Fig. 12, Δt_{td} decreases as the DP moves farther from the distribution substation.

Similarly, under condition P1 (Table III), the DPs were set to B2-1, B2-3, B8-1, and B8-3. The results of the current flowing through CT1 and CT2 calculated using the ATP simulation are shown in Fig. 13. The current phases of I_{CT1} and I_{CT2} changed

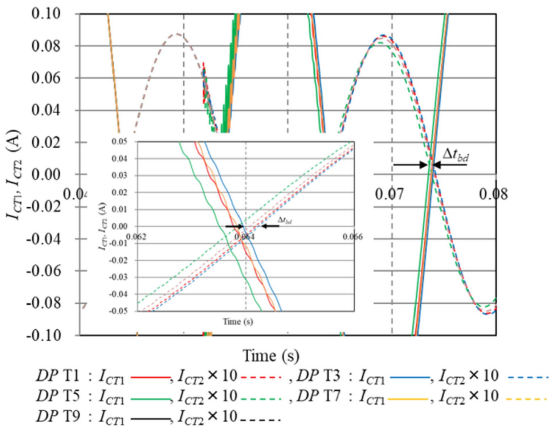

Fig. 13. I_{CT1} and I_{CT2} at the branch line disconnection under condition P1.

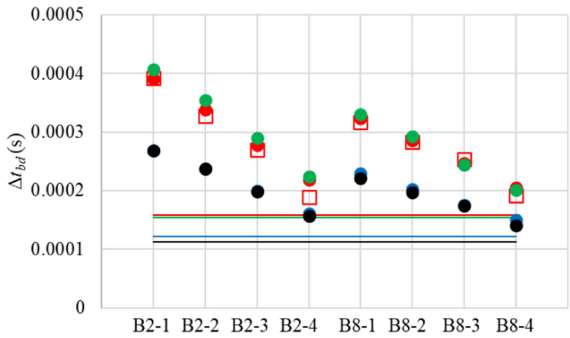

Fig. 14. DP dependency of Δt_{bd} under condition P1.

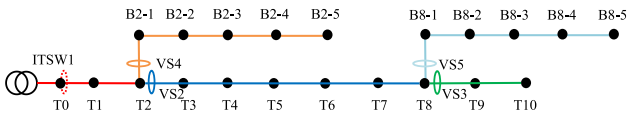

Fig. 15. VS layout and disconnected section identification under condition P1.

before and after the disconnection. Here, the time difference between the zero-crossing points of I_{CT1} and I_{CT2} before and after the disconnection is denoted as the relationship between Δt_{bd} and the DPs is illustrated in Fig. 14. The symbols used for Δt_{bd} are identical to those used for Δt_{td} in Fig. 12. As in the previous case, I_{CT2} was set to a value 10 times that in the simulation. We observed that Δt_{bd} decreased as the distance of the DP from the branch point increased.

Figs. 12 and 14 validate that the DP can be estimated by measuring Δt_{td} and Δt_{bd}, respectively, at the time of disconnection. As shown in Fig. 14, the values of Δt_{bd} are nearly identical when the disconnection occurs in the branch line from B2 and B8, which implies that the DP cannot be accurately identified.

To address this problem, a voltage sensor (VS) was installed on the load side of the branch point at B2 and B8, and the voltage waveform was measured during disconnection to distinguish the disconnected areas at B2 and B8. Fig. 15 displays the recommended VS arrangement, wherein the range of different sensors is ITSW1 (from T1 and T2), VS2 (from the load side of T2 to the power-supply side of T8), VS3 (from the load side of T8 to the end point), VS4 (the branch line of B2), and VS5 (the branch line of B8).

TABLE IV
CALCULATED RESULTS OF R_d AND X_d UNDER P1 CONDITION IN THE TRUNK LINE

DP	1	3	5	7	9
$R_d\,(\Omega)$	24.73	26.87	27.11	27.25	27.47
$X_d\,(\Omega)$	8.61	4.96	4.08	3.28	1.98

TABLE V
CALCULATED RESULTS OF R_d AND X_d UNDER P1 CONDITION IN THE BRANCH LINE

DP	2-1	2-4	8-1	8-4
$R_d\,(\Omega)$	28.42	27.66	24.97	24.71
$X_d\,(\Omega)$	3.97	2.15	2.49	1.49

V. DISCUSSION

Table IV lists the values of X_d and R_d obtained from (2) at the time of disconnection in the trunk line with respect to the DP under the P1 load condition. Table V lists the values of X_d and R_d at the time of branch-line disconnection. Here, V_d and I_d required in (2) represent the voltage in CT2 and the current in CT1 obtained from the ATP simulation conducted on the equivalent circuit shown in Fig. 6, respectively. Table IV indicates that X_d is approximately 15% larger at T9 than that at T1. Conversely, R_d is approximately 109% larger when the DP is at T9 than that at T1. Similarly, Table V validates that the change in X_d is larger than that in R_d.

Fig. 12 illustrates the relationship between $\Delta t_{td\text{-}cal}$ (shown as □) obtained from (1) using X_d and R_d (Table IV) and Δt_{td} obtained from the ATP simulation. Similarly, Fig. 14 illustrates the relationship between $\Delta t_{bd\text{-}cal}$ (shown as □) obtained from (1) using X_d and R_d (Table V) and Δt_{bd} obtained from the ATP simulation. Based on Figs. 12 and 14, we determine that the values of $\Delta t_{td\text{-}cal}$ and Δt_{td} and those of $\Delta t_{bd\text{-}cal}$ and Δt_{bd} are nearly identical. Thus, Δt_{td} and Δt_{bd} are generated based on the changes in X_d and R_d before and after the disconnection.

Tables IV and V indicate that the change in X_d is large relative to the change in R_d. This implies that the change in X_d before and after the disconnection is related to the generation of Δt_{td} and Δt_{bd}. For before and after the disconnection in each section of Fig. 7, x_i should be evaluated because the value of the current changes significantly on power-supply and load sides of the DP; therefore, each section in Fig. 7 is denoted by N in the following discussion.

From (8), x_i is related to the change in L_a. The value of x_i before and after the trunk-line disconnection for each section shown in Fig. 7 is expressed as x_{tN_B} and x_{tN_A}, respectively. Similarly, the value of x_i before and after the branch-line disconnection can be expressed as x_{bN_B} and x_{bN_A}, respectively. Further, N is represented as T01 when N indicates the interval between T0 and T1. If N indicates the distance between B2-1 and

TABLE VI
VALUES OF I_{dNm}, I_{h0Nm}, AND $\cos\theta_{\mathrm{hDN}}$ UNDER P1 CONDITION AT DP T1

(a) After disconnection of the trunk line

N	T01	T34	T56	T78	T910
$I_{dNm}\times10^{-2}$ (A)	0.190	0.151	0.151	0.151	0.072
$I_{h0Nm}\times10^{-3}$ (A)	0.210	0.132	0.110	0.088	0.011
$\cos\theta_{hDN}$	0.641	0.637	0.637	0.638	0.648

(b) After disconnection of the branch line

N	B2-01	B2-45	B8-01	B8-45
$I_{dNm}\times10^{-2}$ (A)	0.039	0.037	0.080	0.081
$I_{h0Nm}\times10^{-2}$ (A)	0.055	0.011	0.055	0.011
$\cos\theta_{hDN}$	0.658	0.634	0.636	0.647

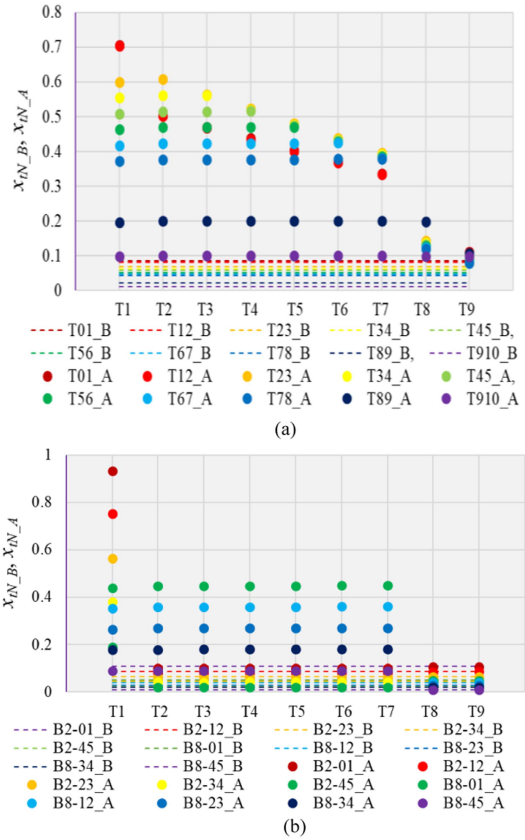

Fig. 16. x_{tN_B} and x_{tN_A} of the trunk and branch lines based on the DP for condition P1 at the time of trunk line disconnection. (a) Trunk line. (b) Branch line.

B2-2 on the branch line from T2, N is represented as B2-12; it is the same for the branch line from T8. Table VI(a) summarizes I_{dNm}, I_{h0Nm}, and $\cos\theta_{hDN}$ of the trunk line at the time of the trunk line disconnection at DP T1 under P1 load conditions. I_{dNm}, I_{h0Nx}, and $\cos\theta_{hDN}$ of the branch line are presented in Table VI(b). Here, I_{dN} and I_{h0N} represent the values obtained from the ATP simulations. Fig. 16(a) illustrates the relationship between the x_{tN_B} and x_{tN_A} of a trunk line obtained from (8) and the DP at the time of the trunk-line disconnection. Fig. 16(b) shows the relationship between x_{tN_B} and x_{tN_A} of the branch

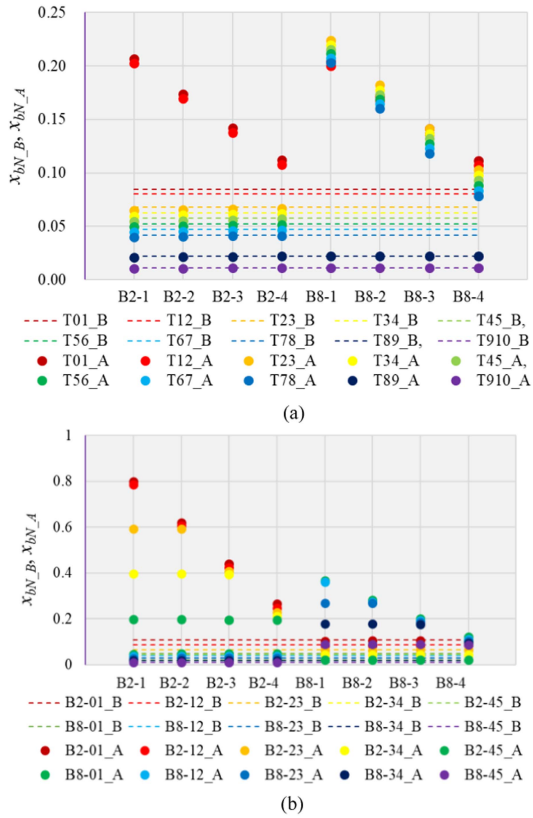

Fig. 17. x_{bN_B} and x_{bN_A} of the trunk and branch lines based on the DP under condition P1 at the time of branch line disconnection. (a) Trunk line. (b) Branch line.

line and the DP. Similarly, Fig. 17(a) illustrates the relationship between x_{tN_B} and x_{tN_A} of the trunk line obtained from (8) and the DP at the time of the branch-line disconnection. Fig. 17(b) illustrates the relationship between x_{bN_B} and x_{bN_A} of the branch line and DP.

We used the results shown in Fig. 16(a) to analyze the tendency of x_{tN_A} to the DP at the time of the trunk-line disconnection. At DP T1, no current flowed in the disconnected phase on the load side from the DP, and therefore, $I_{h0\,T01\,m}$ increased in this section, which in turn increased x_{t01_A}. Conversely, $I_{h0\,T01\,m}$ at the T01 of the DP T9 is smaller than that of DP T1 because the load current flows up to T9. These results suggest that the current imbalance in the T01 section decreases, which reduces $I_{h0\,T01\,m}$. Consequently, x_{t01_A} decreases because of (8). The current flowing in the disconnected phase of the high-voltage line in T01 increases and $I_{h0\,T01\,m}$ decreases because the DP becomes longer. From (8), x_{t01_A} decreases as the DP becomes longer. These results are consistent with the tendency observed in Fig. 16(a). The change in x_{tN_B} at the branch line after the trunk-line disconnection is considered in Fig. 16(b). At DP T1, no current flowed in the branch-line disconnected phase in B2 and B8, and the current imbalance on the starting side of the distribution line increased to a value higher than that on the terminal side. Consequently, both $I_{h0\,Nm}$ and x_{bN_B} increased. At the time of the disconnection from T2 to T7, the branch line from B2 remained unchanged before

and after the disconnection. In addition, the current imbalance increased in the branch line from B8 because no current flowed in the disconnected phase; this phenomenon increased the value of x_{bN_B}. In DPs T9 and T10, the branch lines of B2 and B8 were not influenced by the disconnection. Therefore, x_{bN_B} did not vary before and after their disconnection. Δt_{td} of DP T1 with a large change in L_{aN} ($\sim x_{tN\_A}$) before and after the disconnection from Fig. 16(a) and (b) increases because L_a represents the sum of the acting inductance of each section L_{aN} in Fig. 7. Further, Δt_{td} decreases because the DP becomes longer and the change in L_a after disconnection decreases.

We analyzed the tendency of x_{bN_A} in the trunk line at the time of the branch disconnection using Fig. 17(a). The range of the trunk-line current influenced by DP B2-1 was T01 and T12. At the time of the disconnection at DP B2, the current flowing in the disconnected phase from the branch point increased with an increase in the distance of the DP from the branch point. Therefore, the current imbalance flowing through T01 and T12 decreased with an increase in the distance of the DP from the branch point; the values of x_{b01_A} and x_{b12_A} decreased. In addition, we analyzed the tendency of x_{bN_A} in the branch line at the time of the branch-line disconnection, as depicted in Fig. 17(b). At the time of the disconnection in DP B2-1, no current flowed in the disconnected phase. Therefore, the current imbalance increased, which in turn increased x_{b01_A}. The current flowing through the disconnected phase increased with an increase in the distance from the branch point to the DP; this reduced the current imbalance of B2-01. Thus, x_{bN_A} decreased with an increase in the distance of the DP. Because the branch line from B8 was not influenced by the disconnection at the branch line of B2, x_{bN_B} and x_{bN_A} remained unchanged before and after the disconnection. During the disconnection at the branch line from B8, the tendency remained identical to that observed for the disconnection that occurred at B2. For branch-line disconnections, L_a represents the sum of L_{aN} ($\sim x_{bN\_A}$) in each section, and therefore, Δt_{bd} is larger for B2-1 and B8-1 disconnections, as shown in Fig. 17(a) and (b). In addition, Δt_{bd} decreases with an increase in the DP from the branch point and a decrease in the change in L_a after the disconnection.

Therefore, the results indicated that the change in Δt_{td} and Δt_{bd} after the disconnection could be explained by the change in X_d shown in (4).

VI. Examination of On-Site Applicability

A. Advantages of the Proposed Method

Currently, two methods are used to estimate DPs: (a) a method in which a detection device ITSW is installed on the distribution line to specify the DP [12], [13], [14], and (b) a method using a smart meter [8].

The advantages of the proposed method using an ADL are discussed and compared with the aforementioned methods. Fig. 18 illustrates the method using ITSWs as an example. As shown in Fig. 18, only a few ITSWs can acquire the voltage and current information in a distribution line. For instance, when a disconnection occurs between ITSW2 and ITSW3, the voltage information of ITSW2 on the power-supply side of the DP and ITSW3 after the DP reveals that the disconnected section is between them. The proposed ADL-based method, which can be used to estimate the DP of the trunk and branch line instead of the disconnected section from the time difference of the zero-crossing points, is illustrated in Figs. 12 and 14.

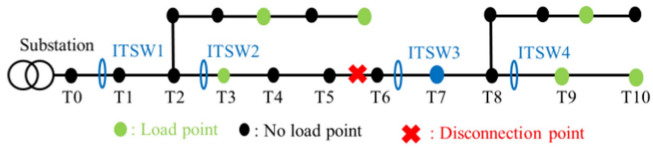

Fig. 18. Concept of disconnection detection methods using a smart meter or ITSW.

The method using smart meters is illustrated in Fig. 18. We assumed that smart meters are installed at different locations (load points). For example, if the DP occurs between T5 and T6, no abnormal voltage is generated in the smart meter at T3 on the power-supply side of the DP; however, an abnormal voltage is generated at the end side of the DP. This result indicates that the disconnected section is on the terminal side of T3. The proposed method can estimate DPs regardless of the presence of a smart meter, as shown in Figs. 12 and 14. The installation of the ITSW can be omitted if the voltage information obtained from the VS proposed in this method can be replaced by the information obtained from the smart meter. The disconnected section can be narrowed down by the smart meter, and the DP can be identified using the proposed method, thereby improving the cost-effectiveness.

B. Application of Proposed Method to Actual Equipment

To apply the proposed method in practice, a prior simulation is necessary to link the time difference between the zero-crossing and the DP. The management of distribution-line facilities is increasingly performed within systems such as servers, and therefore, highly accurate simulations are expected when using these facility data. The steps for the application of the proposed method to a real field are as follows:

Step 1: The relationship between Δt_{td} and Δt_{bd} is determined with respect to DP by simulation using the load bias of the target distribution line as a parameter.

Step 2: The disconnected section is identified by obtaining voltage information from VS information.

Step 3: Δt_{td} or Δt_{bd} are calculated from the time difference between I_{CT1} and I_{CT2} at the time of the disconnection.

Step 4: Δt_{td} or Δt_{bd} obtained at the time of disconnection and the result obtained in Step 1 are compared to estimate the DP.

The DP can be estimated using this procedure. The current values in distribution lines change as the use of electricity changes during the day. This method is applicable even when the current flowing in the distribution line is approximately halved [10]. V_d in Fig. 6 depends on the magnitude of I_{h0}, and as I_{h0} decreases, V_d decreases, resulting in a relationship where I_d also decreases. From (8), the reason for the occurrence of Δt_{td} and Δt_{bd} can be attributed to x_i, which is an element of L_a. I_{dm} and $I_{h0\,m}$ both decrease with a decrease in the current flowing in the high-voltage line. Therefore, x_i does not depend only on the magnitude of the high-voltage-line current.

We examined the time resolution of the ammeters (CT1 and CT2) required to construct the system. The distance between the utility poles was approximately 40 m, and based on our field experience, we determined that an estimation accuracy of approximately 100 m (two to three utility poles) would be required to reduce the time required to identify the DP. By comparing Figs. 12 and 14, the value of Δt_{td} per km at the time of the trunk-line disconnection was found to be smaller than that at the time of the branch-line disconnection.

As the DP increased by 1 km, Δt_{td} decreased by approximately 4×10^{-5} s. The minimum time resolution required to estimate the DP with an accuracy of 100 m was 4×10^{-6} s, which was 1/10 of 1 km. To improve the measurement accuracy, the time resolution was set to 1.0×10^{-6} s, which was half of 2×10^{-6} s truncated.

We developed a sensor switch that can realize time synchronization with a measurement frequency of several megahertz to ensure the time synchronization of CT1 and CT2. We used this switch to apply the method of using the time difference between the arriving ground-fault surge currents to the ground-fault point estimation of distribution lines. Furthermore, the time of the ammeters can be synchronized using a GPS.

VII. Conclusion

We developed an efficient DP estimation method using an ADL for long-distance distribution lines with branched lines. The proposed method requires the installation of ADL and VS equipment and two time-synchronized ammeters and estimates the point of disconnection from the time difference between the rise of the distribution line after the disconnection and the zero-crossing point of the current flowing through the two ammeters installed at the end of the line. Communication facilities must be constructed to transfer measurements of I_{CT1} and I_{CT2}. This method can be applied to general-purpose products that do not require the development of new equipment. Especially, in the case of distribution lines in rural areas over long distances, it takes significant time to determine the DP; therefore, it can be concluded that the proposed method, which can be constructed using general-purpose products, can effectively reduce the time required to identify the DP.

Furthermore, we investigated the factors that cause the time difference between the zero-crossing points before and after the disconnection. The procedure for applying the proposed method to the actual equipment and the time resolution required for the ammeters were analyzed. The proposed method can be used to achieve early DP detection, which can reduce power outage time and ensure public safety.

The proposed method should be validated in a facility close to the actual site to evaluate its field applicability in the future. To explore the applicability of the proposed method, the impact of load distribution in distribution lines needs to be evaluated, and the load magnitude should be varied at each point. The applicability of the proposed method in an event in which the load is randomly set also needs to be assessed.

We confirmed that the fault-point estimation method using the ADL could be applied to ground faults, short circuits, and the disconnection of distribution lines by ATP simulations; further, the proposed method can be considered an efficient maintenance method for distribution lines.

Acknowledgment

The authors thank Mr. Y. Nishida of TEPCO Holdings, Inc., Mr. R. Yamamoto, and the researchers at Waseda University for their assistance in conducting this study.

We would like to thank Editage (www.editage.com) for English language editing.

References

[1] Electric Technology Research Association, "Advancement of distribution automation system technology," *Electron. Technol. Res.*, vol. 67, no. 2, pp. 113–118, 2011.

[2] M. Pourahmadi-Nakhli and A. A. Safavi, "Path characteristic frequency-based fault locating in radial distribution systems using wavelets and neural networks," *IEEE Trans. Power Del.*, vol. 26, no. 2, pp. 772–781, Apr. 2011.

[3] Y. Kodama, M. Watanabe, and N. Maeda, "Validity verification for estimating ground fault locations by simulator of reproduce ground fault," *IEEJ Trans. Power Energy*, vol. 137, no. 5, pp. 102–109, Feb. 2017.

[4] Y. Kodama, R. Yamamoto, Y. Nishida, and T. Sano, "Branch point estimation leading to ground fault location using ground fault current flowing to common earthing conductor," *IEEJ Trans. Power Energy*, vol. 138, no. 9, pp. 772–780, Sep. 2018.

[5] Q. H. Alsafasfeh, "Pattern recognition for fault detection, classification, and localization in electrical power systems," Ph.D. dissertation, Dept. Elect. Comput. Eng., Western Michigan Univ., Kalamazoo, MI, USA, 2010.

[6] F. Han, X. Yu, M. Al-Dabbagh, and Y. Wang, "Locating phase-to-ground short-circuit faults on radial distribution lines," *IEEE Trans. Ind. Electron.*, vol. 54, no. 3, pp. 1581–1590, Jun. 2007.

[7] Y. Kodama and Y. Hayashi, "Short-circuit point estimation method using abnormal detection line of distribution line," *IEEJ Trans. Elect. Electron. Eng.*, vol. 17, pp. 1452–1459, Oct. 2022.

[8] S. Kitamura, T. Takano, Y. Izui, and N. Itaya, "Disconnection detection method for power distribution lines using smart meters," in *Proc. IEEE Power Energy Soc. Innov. Smart Grid Technol. Conf.*, 2015, pp. 1–5.

[9] Z. Qi, T. Yingjie, S. Yun, Q. Haini, and G. Naiwang, "Ungrounded fault detection in medium voltage distribution network based on machine learning," in *Proc. IEEE 2nd Conf. Energy Internet Energy Syst. Integration*, 2018, pp. 1–5.

[10] Y. Kodama, Y. Hayashi, and N. Nishida, "Estimation method of disconnection point using common earthing conductor for distribution line without branch line," *IEEJ Trans. Power Energy*, vol. 141, no. 8, pp. 559–567, Aug. 2021.

[11] Y. Kodama, Y. Hayashi, and N. Nishida, "Estimation method of disconnection point using common earthing conductor for distribution line with branch line," *IEEJ Trans. Power Energy*, vol. 142, no. 1, pp. 34–40, 2022.

[12] Q. Kang et al., "Analyses and judgment methods of single-phase broken-line fault for loaded distribution line," in *Proc. IEEE PES Asia-Pacific Power Energy Conf* ., 2016, pp. 482–486.

[13] D. Jia, K. Liu, X. Meng, and X. Song, "Location of single phase disconnection fault with non-grounding in distribution grid based on positive sequence voltage," in *Proc. IEEE Int. Conf. Renewable Power Gener.*, Beijing, 2015, pp. 1–6, doi: 10.1049/cp.2015.0567.

[14] Z. Wang, Z. Gao, M. Zheng, J. Yu, and P. Zong, "Protection in active distribution network against short circuit fault and broken line fault," in *Proc. IEEE 4th Conf. Energy Internet Energy Syst. Integration*, 2020, pp. 1685–1690.

[15] Z. Qiqi, L. Siyi, and Z. Yan, "Power distribution network disconnection fault diagnosis using data mining method," in *Proc. IEEE PES Innov. Smart Grid Technol. Asia*, 2019, pp. 407–411.

[16] Z. Qi, S. Yun, G. Naiwang, T. Yingjie, and Q. Haini, "Ungrounded fault detection in medium voltage distribution network based on machine learning," in *Proc. IEEE 2nd Conf. Energy Internet Energy Syst. Integration*, 2018, pp. 1–5.

[17] A. Pongthavornsawad and W. Rungseevijitprapa, "Broken conductor detection for overhead line distribution system," in *Proc. IEEE Asia-Pacific Power Energy Eng. Conf.*, 2011, pp. 1–4.

Yasuhiro Kodama received the B.Sc. degree from Meiji University, Tokyo, Japan, and the M.Eng. degree from Tsukuba University, Tsukuba, Japan, in 1994 and 1996, respectively, and the D.Eng. degree from Yokohama National University, Yokohama, Japan, in 2018.

In 1997, he joined Tokyo Electric Power Company, Inc., Tokyo, Japan, where he worked in maintenance management and research and development of distribution lines. He became a Researcher with the Advanced Collaborative Research Organization for Smart Society, Waseda University, Tokyo, Japan, in October 2020. His research interests include power quality in distribution systems with large distributed energy resources.

Dr. Kodama is the Member of the Institute of Electrical Engineers of Japan and of CIGRE SC C6 (Distribution Systems and Dispersed Generation).

Yasuhiro Hayashi (Member, IEEE) received the B.Eng., M.Eng, and D.Eng. degrees from Waseda University, Tokyo, Japan, in 1989, 1991, and 1994, respectively.

In 1994, he became a Research Associate with Ibaraki University, Mito, Japan. In 2000, he became an Associate Professor with the Department of Electrical and Electronics Engineering, Fukui University, Fukui, Japan. Since 2009, he has been a Professor with the Department of Electrical Engineering and Bioscience, Waseda University and Director of the Research Institute of Advanced Network Technology since 2010. Since 2014, he has been the Dean of the Advanced Collaborative Research Organization for Smart Society with Waseda University. His research interests include the optimization of distribution system operation and the forecasting, operation, planning, and control related to renewable energy sources and demand response.

Dr. Hayashi is the Senior Member of the Institute of Electrical Engineers of Japan and Regular Member of CIGRE SC C6 (Distribution Systems and Dispersed Generation).